Applied Catalysis A, General 710 (2026) 120670

Contents lists available at ScienceDirect

Applied Catalysis A, General

journal homepage: www.elsevier.com/locate/apcata

# Catalysts for unlocking $H_2$ production from $NH_3$: A process design perspective

Elvira Spatolisano, Federica Restelli, Giorgia De Guido, Stefania Moioli, Laura A. Pellegrini *

*GASP - Group on Advanced Separation Processes & GAS Processing, Dipartimento di Chimica, Materiali e Ingegneria Chimica "G. Natta", Politecnico di Milano, Piazza Leonardo da Vinci 32, Milano 20133, Italy*

ARTICLE INFO

*Keywords:*
H2 carrier
Energy vector
Process intensification
Net-zero CO2 emissions

ABSTRACT

$NH_3$ cracking is gaining attention as a promising route for on-demand, carbon-free $H_2$ production, particularly in off-grid or distributed energy applications. Nevertheless, its practical implementation hinges on the development of catalysts not only highly active, but also cost-effective and thermally efficient. Starting from the state-of-the-art catalyst for $NH_3$ decomposition (nickel-based), the most promising catalytic systems (ruthenium-based) are critically reviewed, with a focus on the interplay between catalyst activation energy, thermal duty and operating conditions. In view of discussing whether the implementation of noble-based catalysts can be practical or not, a technical analysis of the cracking furnace with different Ru-based catalytic systems is presented, referring to a decentralized application representative of compact yet industrially relevant units. The trade-off between technical and economic performance is quantified, with the aim of offering design guidelines for developing scalable $NH_3$ cracking.

## 1. Introduction

Ammonia cracking has emerged as a critical technology in the transition to a sustainable, hydrogen-based energy economy [1]. However, for $NH_3$ to be used as a $H_2$ source, particularly in mobility sector applications requiring high-purity hydrogen [2], it must first be cracked into its elemental gases.

This decomposition reaction is thermodynamically favourable at high temperatures but kinetically slow without a catalyst. Therefore, active catalysts play a pivotal role in enhancing the rate of ammonia cracking at practical temperatures [3]. The choice of catalyst directly influences the efficiency, energy consumption and feasibility of the cracking process.

Catalysts used for ammonia decomposition include noble metals, non-noble metals, bimetallic compounds, nitrides and carbides [4]. Among these, ruthenium (Ru)-based catalysts demonstrate the highest catalytic activity at low temperatures [5]. However, the high cost of Ru significantly restricts its widespread industrial use.

To mitigate this limitation, researchers have explored the development of bimetallic catalysts by combining Ru with more economical transition metals such as nickel (Ni) and iron (Fe). These combinations leverage synergistic effects to improve catalytic efficiency while reducing overall costs [6]. Nevertheless, due to the inherent complexity of bimetallic catalyst synthesis and surface characteristics, further research is necessary to precisely control their structure and composition to achieve optimal performance.

In contrast to noble metals, non-noble metal catalysts, including Ni, Fe and Co, are more economically viable. Among these, Ni-based catalysts earned considerable interest in industrial ammonia decomposition due to their favourable cost and catalytic performance, which is second only to Ru-based systems. Efforts to enhance the activity and thermal stability of Ni-based catalysts under low-temperature and low-pressure conditions often involve doping with secondary metals to improve dispersion and metal-support interactions, thereby boosting overall catalytic efficiency [7].

As nickel-based catalysts are widely recognized as the state-of-the-art of ammonia cracking, while ruthenium remains the gold standard for it, these two options are deepened in Section 2, while $NH_3$ cracking mechanism is briefly reviewed in Section 3.

With the aim of offering a valuable framework to guide research efforts toward catalysts design for their viable industrial application, a preliminary techno-economic analysis of $NH_3$ cracking furnace is

* Corresponding author.
*E-mail address:* laura.pellegrini@polimi.it (L.A. Pellegrini).

https://doi.org/10.1016/j.apcata.2025.120670
Received 25 June 2025; Received in revised form 28 August 2025; Accepted 1 November 2025
Available online 4 November 2025

presented. Considering different Ru-based catalysts, the interplay between activation energy, thermal duty and operating conditions is examined and compared with the Ni benchmark. As a result, performance indicators required for Ru-based catalysts to match or exceed the $NH_3$ decomposition efficiency of the Ni-based alternative are identified. These performance thresholds, together with highlighting the trade-offs between catalytic activity, energy requirements and cost, can contribute to a deeper understanding of the operating and economic parameters necessary for scaling ammonia cracking technologies, particularly in decentralized $H_2$ production scenarios.

## 2. State-of-the-art and future ammonia cracking catalysts

Some of the ammonia cracking catalysts are already available commercially and are mostly Ni-based, as shown in Table 1.

### 2.1. State-of-the-art of $NH_3$ cracking: Ni-based catalysts

Nickel is among the most extensively studied non-noble metal catalysts for ammonia decomposition due to its favourable catalytic activity and low cost. As the second most active metal after ruthenium, Ni-based catalysts are already commercial for large-scale and economically viable hydrogen production.

Nevertheless, compared to Ru-based catalysts, Ni-based systems generally require higher reaction temperatures to achieve a comparable $NH_3$ conversion. This limitation is primarily attributed to the lower intrinsic activity of Ni for the nitrogen desorption step, often identified as the rate-determining step in the reaction mechanism.

To enhance the performance of Ni-based catalysts, researchers have employed several strategies, including the following.

- Support modification. The choice of support material plays a critical role in influencing Ni dispersion, particle size, and metal-support interactions. Common supports include $Al_2O_3$, MgO, $SiO_2$ and carbon-based materials. Basic support, such as MgO, can enhance electron density around Ni active sites, facilitating ammonia activation and improving catalytic efficiency. Appropriate support not only ensures uniform dispersion of Ni particles but also enhances their stability and interaction with reactant molecules through its acid-base characteristics. This, in turn, helps prevent sintering and early deactivation, thereby prolonging the catalyst's lifespan and improving the performance of Ni-based catalysts [7].

- Promoter addition. Alkali and alkaline earth metals such as K, Cs and Sr are often introduced as promoters. These elements donate electrons to the Ni surface, which facilitates nitrogen desorption by weakening the Ni–N bond. Additionally, promoters can modify the acid-base properties of the support and suppress the formation of inactive Ni species.

- Bimetallic and alloy formation. Combining Ni with other transition metals such as Fe, Co, or Cu can induce synergistic effects that improve activity, selectivity, and thermal stability. These combinations can alter the electronic structure of Ni, enhance its resistance to sintering, and improve catalyst longevity under harsh reaction conditions.
- Nanostructuring and morphological control. The development of Ni-based catalysts with controlled morphologies (nanowires, nanospheres or core-shell structures) has shown potential for increasing surface area and active site accessibility. These structures also contribute to improved thermal stability and resistance to deactivation.

Despite the quite mature technology, challenges remain in enabling low-temperature operation and long-term stability of Ni-based catalysts. Deactivation due to sintering, nitrogen poisoning and support degradation can significantly reduce catalyst's lifespan.

Table 2 offers a summary of the most recent literature discussing the experimental evaluation of Ni-based catalysts for $NH_3$ cracking, considering operating conditions, activity and apparent activation energy.

As a general remark, catalysts with lower apparent activation energy exhibit higher reaction rates at a given temperature, thereby demonstrating greater activity. This enhanced activity allows the reaction to proceed at reduced operating temperatures while maintaining high conversion levels. Consequently, the thermal duty required to sustain the process is significantly lowered. This relationship is especially critical in endothermic systems, as the $NH_3$ cracking case-study. Therefore, the development of highly active catalysts with low activation energy is not only essential for improving reaction kinetics but also for minimizing energy consumption, enabling cost-effective $H_2$ production from $NH_3$. In this respect, to critically analyse the outcomes of the experimental activities of Table 2, Fig. 1 provides an overview of the apparent activation energy of each Ni-based catalyst, depending on the supports analysed, also considering active phase loading.

Overall, the apparent activation energies for these systems ranges from 40 to 100 kJ/mol. Ce-modified $Al_2O_3$ supports show the lowest value of $E_{app}$, for a Ni loading of 10 wt%. On the other hand, the highest values are registered for $SrNiO_{3-\delta}$-600$H_2$ and $La_{0.2}Sr_{0.8}NiO_{3-\delta}$-600$H_2$ supported catalyst, also having the highest amount of active phase dispersed on the support (around 29 wt% and 27 wt%, respectively).

In addition, Fig. 2 provides $NH_3$ conversion ($\chi$) both as a function of temperature and active phase loading. The different catalytic activities experienced at same temperatures and same loadings confirm the structure-sensitive nature of the $NH_3$ cracking reaction. Ce-modified $Al_2O_3$ supported catalysts, if compared with H-ZSM-5 zeolite catalysts, present lower $NH_3$ conversion despite the doubled Ni loading. This evidence can be due to the appropriate interaction between Ni particles and ZSM-5 support [5].

**Table 1**
Summary of commercially available $NH_3$ cracking catalysts.

| Supplier | Catalyst name | Active phase | $T$ [°C] | Applications |
|---|---|---|---|---|
| BASF [8] | SYNSPIRE™ ARC series 2 | ruthenium | 280–580 | not reported |
| | SYNSPIRE™ ARC series 6 | nickel | 420–640 | |
| | SYNSPIRE™ ARC series 8 | nickel | 620–800 | |
| Johnson Matthey [9] | KATALCO™ 27–2 | nickel | 700–950 | large-scale $H_2$ production for industrial application (>1000 MTPD $NH_3$) |
| | KATALCO™ 27–612 | Platinum Group Metals (PGM) | 400–500 | decentralized $H_2$ generation (>100 kg/h $NH_3$) |
| Clariant [10] | HyProGen™ 820 DCARB | nickel | 400–650 | adiabatic reactors |
| | HyProGen™ 830 DCARB | nickel | 550–750 | reformer-type fired tubular reactors |
| | HyProGen™ 850 DCARB | ruthenium | 370–550 | small-scale, decentralized applications |
| Topsoe [11] | DNK−2R | iron-cobalt | | 100–3400 MTPD $NH_3$ single-line capacity range |
| | DNK−20 | nickel | | |
| | DNK−30 | nickel | | |

**Table 2**
Summary of most recent literature on experimental evaluation of Ni-based catalyst for $NH_3$ cracking.

| Name | Support | Loading [wt%] | $T$ [°C] | $P$ [bar] | $GHSV$ [mL $h^{-1}$ $g_{cat}^{-1}$] | $NH_3$ conversion [%] | $H_2$ production rate [mmol $min^{-1}$ $g_{cat}^{-1}$] | $E_{app}$ [kJ $mol^{-1}$] | Reference |
|---|---|---|---|---|---|---|---|---|---|
| Al-oxides | Mg-Al-O | 20 | 450 | 1 | 6000 | 6.7 | | 89.3 | Im et al. |
| | Ca-Al-O | 20 | 450 | 1 | 6000 | 11.5 | | 87.2 | [12] |
| | Sr-Al-O | 20 | 450 | 1 | 6000 | 16.5 | | 81.1 | |
| | Ba-Al-O | 20 | 450 | 1 | 6000 | 24.8 | | 76.5 | |
| Ce-modified $Al_2O_3$ | $Al_2O_3$ | 9.6 | 500 | 1 | 6000 | 43 | 2.9 | 84.2 | Do et al. |
| | $Al_1Ce_{0.05}O_x$ | 9.6 | 500 | 1 | 6000 | 76 | 5.1 | 74.7 | [13] |
| | $Al_1Ce_{0.05}O_x$ | 19.3 | 500 | 1 | 6000 | 84.9 | 5.7 | – | |
| | γ-$Al_2O_3$ | 10 | 650 | | 30,000 | 30 | 9.73 | 70.9 | Yu et al. |
| | $Al_{0.75}Ce_{0.25}O_x$ | 10 | 650 | | 30,000 | 55 | 18.31 | 50.58 | [14] |
| | $Al_{0.5}Ce_{0.5}O_x$ | 10 | 650 | | 30,000 | 65 | 21.79 | 40.98 | |
| | $Al_{0.25}Ce_{0.75}O_x$ | 10 | 650 | | 30,000 | 52 | 17.48 | 46.23 | |
| $La_2O_3$ | $LaNiO_{3-\delta}$-600$H_2$ | 25.5 | 550 | 1 | 30,000 | 48.7 | 16.3 | 85.1 | Guo et al. |
| | $La_{0.5}Sr_{0.5}NiO_{3-\delta}$-600$H_2$ | 25.6 | 550 | 1 | 30,000 | 87.7 | 29.4 | 97.2 | [15] |
| | $La_{0.2}Sr_{0.8}NiO_{3-\delta}$-600$H_2$ | 26.8 | 550 | 1 | 30,000 | 66.5 | 22.3 | 104.7 | |
| | $SrNiO_{3-\delta}$-600$H_2$ | 28.6 | 550 | 1 | 30,000 | 48.9 | 16.4 | 106.4 | |
| Graphene aerogel | rNiGA-$NiNO_3$ | 11.4 | 600 | 1 | 30,000 | 55.4 | 17 | 100.7 | Kocer et al. |
| | rNiGA-$NiNO_3$-EA | 9.3 | 600 | 1 | 30,000 | 63.3 | 19.4 | 103.7 | [16] |
| | rNiGA-Ni(acac)$_2$ | 11.1 | 600 | 1 | 30,000 | 70.2 | 21.6 | 94.8 | |
| H-ZSM−5 zeolite | ZSM−5(MSSIE) | 5 | 650 | | 30,000 | 97.6 | 32.7 | 88.1 | Hu et al. |
| | ZSM−5(SSIE) | 5 | 650 | | 30,000 | 92.9 | 31.1 | 97.7 | [17] |
| | ZSM−5(DP) | 5 | 650 | | 30,000 | 81.3 | 27.2 | 98.1 | |
| | ZSM−5(IM) | 5 | 650 | | 30,000 | 50.1 | 16.8 | 98.2 | |

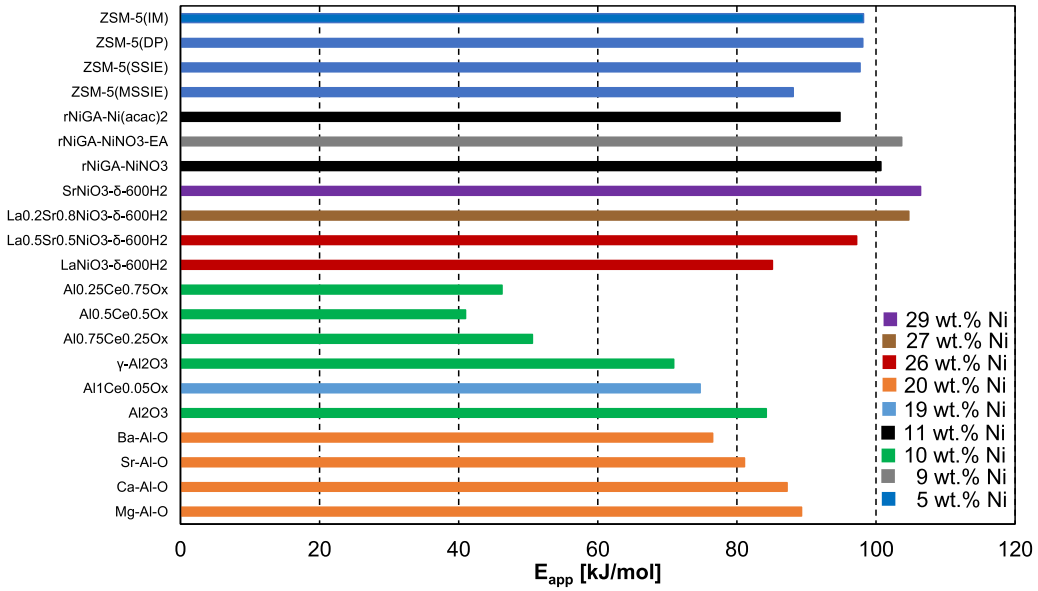


**Fig. 1.** Apparent activation energy ($E_{app}$) of Ni-based catalysts of Table 2.

### 2.2. Future of $NH_3$ cracking: Ru-based catalysts

Ruthenium is widely recognized as the most active metal for ammonia decomposition, exhibiting superior catalytic performance even at moderate temperatures (400–500°C) compared to other transition metals. Its exceptional activity, particularly at lower temperatures, is primarily attributed to its optimal balance of adsorption energies for ammonia and its decomposition intermediates, as well as its high intrinsic activity for nitrogen desorption, *i.e.,* the rate-limiting step in the reaction mechanism.

However, ruthenium is one of the rarest metals, typically found in platinum ores and recovered as a byproduct of nickel and platinum refining. While demand is increasing, supply remains constrained, creating a structural mismatch between industrial needs and scalable availability. As recognition of its strategic importance grows, securing future supply will require stronger recycling systems and diversified recovery pathways in view of its reliable industrial application.

Significant research efforts have been devoted to improving the atom efficiency and catalytic performance of Ru while minimizing its loading.

To address these limitations, ongoing research is focused on optimizing support–metal interactions, developing low-Ru or Ru-free alternatives with comparable activity, and exploring regeneration strategies to prolong catalyst's lifetime.

Table 3 summarizes the most recent experimental studies on Ru-based catalysts available in literature.

With the aim of an overall review of the experimental results, Fig. 3 shows the apparent activation energy of Ru-based catalysts of Table 3, considering $Al_2O_3$ supported, MgO supported, rare earth supported and other tested catalytic systems.

Also in this case, high variability is experienced depending on the support, with the apparent activation energy ranging from 65 to around 200 kJ/kmol, this very high value achieved for the MgO supported catalyst. For Mg-based supports, the apparent activation energy ranges from 70 to 210 kJ/mol, with the lowest value shown for the K-promoted

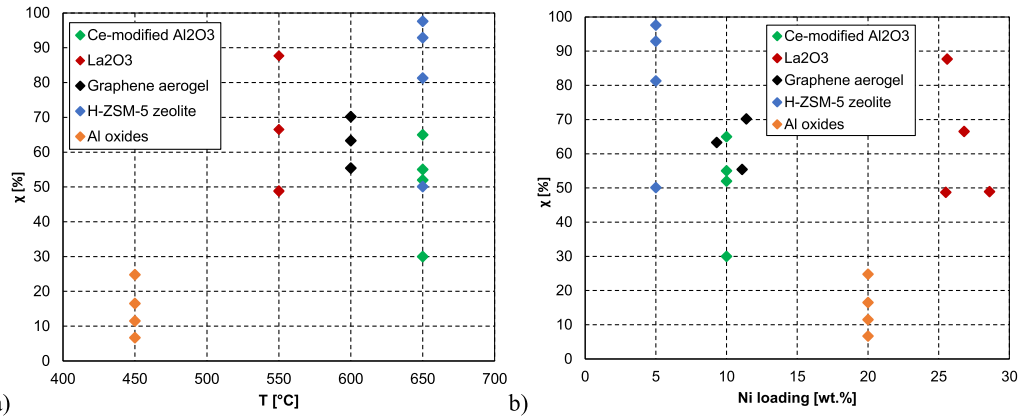


**Fig. 2.** $NH_3$ conversion ($\chi$) for some of the Ni-based catalysts of Table 2 explored in literature, as a function of: a) temperature ($T$) and b) Ni loading. *GHSV* is fixed at 30000 mL $h^{-1}$ $g_{cat}^{-1}$.

MgO supported catalyst proposed by Sayas et al. [23]. Indeed, the alkaline promoter is beneficial for improving the catalytic performance of $NH_3$ cracking. Nevertheless, research on the promoting mechanism is still not mature enough and results are controversial.

On the other hand, trivalent rare earth oxides ($RE_2O_3$) exhibit excellent performance in ammonia decomposition reaction even at low operating temperatures ($T = 450$ °C), as also shown in Fig. 4.

Xu et al. [19] suggested that the $RE_2O_3$ with intrinsic surface $O_v$ promoted the adsorption and activation of the catalyst on Lewis basic reactant molecules and enhanced the interaction between the active metals and the rare earth oxide supports, raising the *d* band of Ru and increase the energy of surface adsorbed $NH_2$. As a result, these catalytic species offer moderate adsorption of $NH_3$, maintaining active species in metallic state and forming unique RE-N-H-Ru configurations for the N-H bond breaking.

### 2.3. Kinetics of $NH_3$ decomposition

$NH_3$ decomposition involves adsorption, stepwise dehydrogenation and recombination, as in Eq. (1) to (4) (* stands for the catalyst active site) [34].

$$NH_3 + * \leftrightarrow NH_3^* \qquad r_1 = \vec{k_1} y_{NH_3} \vartheta - \overleftarrow{k_1} \vartheta_{NH_3^*} \tag{1}$$

$$NH_3^* + * \rightarrow NH_2^* + H^* \qquad r_2 = \vec{k_2} \vartheta_{NH_3^*} \vartheta^3 \tag{2a}$$

$$NH_2^* + * \rightarrow NH^* + H^* \tag{2b}$$

$$NH^* + * \rightarrow N^* + H^* \tag{2c}$$

$$2N^* \rightarrow N_2 + 2* \qquad r_3 = \vec{k_3} \vartheta_{N^*}^{\ 2} \tag{3}$$

$$H^* + H^* \leftrightarrow H_2 + 2* \qquad r_4 = \vec{k_4} \vartheta_{H^*}^{\ 2} - \overleftarrow{k_4} y_{H_2} \vartheta^2 \tag{4}$$

The rate-determining step (RDS) for ammonia decomposition differs slightly between Ru and Ni catalysts due to differences in their surface binding energies. For Ru-based systems, the RDS is widely supposed to be nitrogen recombination. Ru strongly binds nitrogen atoms (N*), but the recombination and desorption of $N_2$ gas is energetically demanding. First-principles and experimental studies consistently identify this as the slowest step [5].

For Ni-based catalysts, the RDS can be either nitrogen recombination or one of the earlier $NH_x$ dehydrogenation steps, depending on temperature and hydrogen partial pressure.

Ni binds hydrogen more strongly than Ru, so surface H* coverage can be high. This evidence can lead to hydrogen poisoning of the catalyst surface, which may slow dehydrogenation steps. Under hydrogen-rich conditions, the dehydrogenation from $NH_2$* to NH* can become rate-limiting [35].

One of the first attempts to derive a detailed kinetic model of $NH_3$ decomposition on Ru and Ni catalysts was made by Takahashi and Fujitani [34]. They found that kinetic constants for $NH_3$ dehydrogenation over Ru-based catalyst was about 1 order of magnitude higher than over Ni catalyst. In contrast, the kinetic constant for recombinative $N_2$ desorption for Ru catalyst was ½ that over Ni catalyst. These results suggested that $N_2$ recombination step is faster on Ni catalysts, while reactions on the surface involving $H_2$ are assumed to proceed more readily on the Ru catalysts.

Since then, few references have been published in literature trying to draw conclusions on kinetics, as a follow up of the experimental testing. Rate expressions are mostly empirical and usually follow the Temkin–Pyzhev kinetics. Table 4 provides an overview of kinetic modelling proposed in literature for Ni- and Ru-based catalysts of Table 2 and Table 3. Usually, the reaction order for $N_2$ is assumed to be zero for all the catalysts, meaning that $N_2$ adsorption is extremely weak at such low total pressures, typical of $NH_3$ cracking. On the other hand, the reaction order for $NH_3$ partial pressure was a positive value at the reaction conditions for all the catalysts but for $Ru/TiO_2$-500N-6h. According to Yan et al. [32], this negative α-value manifests that the dissociation of N–H bonds is inhibited because of the nitridation of $TiO_x$ species, considered unfavourable for the dissociation of N–H bonds.

In contrast, the reaction order for $H_2$ partial pressure was negative for all the catalysts. Hydrogen exhibits the inhibitory effect on $NH_3$ decomposition as adsorbed $H_2$ occupies the active sites. Im et al. [12] suggested that the strong basic property of the catalysts can alleviate this $H_2$ inhibitory effect, as proved by the increasing $H_2$ reaction order with increased basic strength. In addition, Qiu et al. [24] showed that first order on $NH_3$ kinetic dependences and −1.5 on $H_2$ are in line with the assumption

that the rate determining step is the $NH_3$ dehydrogenation, excluding the hypothesis of associative desorption of $N_2$, which would imply a quadratic dependence on $NH_3$ and the negative order −3 with respect to $H_2$.

To analyse the predictions of the rate expressions of Table 4 consistently, a pseudo-homogeneous 1-D isothermal packed bed reactor has been simulated, at variable temperature and with different Ni- and Ru-based catalyst particles. The space velocity is fixed at 6 $m^3/h/kg_{cat}$, pure $NH_3$ is assumed as the feed stream, while the catalyst mass is 300 kg for all the case-studies. Where parameters of the Temkin–Pyzhev kinetics were not provided by the references considered (typically, the pre-exponential factor, $k_0$), they were regressed against available experimental data. Details about experimental data fitting are provided in section S1.

Fig. 5 offers an overview of the $NH_3$ conversion ($\chi$) for Ni- and Ru-

**Table 3**
Summary of most recent literature on experimental evaluation of Ru-based catalyst for $NH_3$ cracking.

| Name | Support | Loading [wt%] | T [°C] | P [bar] | GHSV [mL $h^{-1}$ $g_{cat}^{-1}$] | $NH_3$ conversion [%] | $H_2$ production rate [mmol $min^{-1}$ $g_{cat}^{-1}$] | $E_{app}$ [kJ/mol] | References |
|---|---|---|---|---|---|---|---|---|---|
| rare earth oxide | $Sm_2O_3$-p | 3.8 | 450 | 1 | 30,000 | 84.6 | 25.9 | 85.1 | Zhang et al. |
| | $Sm_2O_3$-i | 3.7 | 450 | 1 | 30,000 | 21.5 | 6.6 | 96 | [18] |
| | $Sm_2O_3$-m | 3.5 | 450 | 1 | 30,000 | 15.7 | 4.9 | 100.2 | |
| | $Sm_2O_3$ | 1.03 | 450 | | 30,000 | 72 | 24 | 102.2 | Xu et al. |
| | $Sm_2O_3$ | 1.03 | 450 | | 300,000 | | 138.2 | | [19] |
| | $Y_2O_3$ | 1.06 | 450 | | 300,000 | | 124.9 | | |
| | $Y_2O_3$ | 1.06 | 450 | | 30,000 | | 20.4 | 123.5 | |
| | $Gd_2O_3$ | 0.82 | 450 | | 300,000 | | 103.4 | | |
| | $Gd_2O_3$ | 0.82 | 450 | | 30,000 | | 21.4 | 105.1 | |
| | $Pr_6O_{11}$ | 4.7 | 450 | 1 | 30,000 | 16.6 | 5.1 | 87.2 | Zhang et al. |
| | $Pr_2O_3$ | 4.8 | 450 | 1 | 30,000 | 68.2 | 20.9 | 66.3 | [20] |
| La-Ce-based | $Ce_1$ | 1.8 | 400 | 1 | 6000 | | 5.1 | 91 | Le et al. |
| | $La_{0.09}Ce_{0.91}$ | 1.9 | 400 | 1 | 6000 | 79 | 5.1 | | [21] |
| | $La_{0.2}Ce_{0.8}$ | 1.9 | 400 | 1 | 6000 | 82 | 5.6 | | |
| | $La_{0.33}Ce_{0.67}$ | 1.8 | 400 | 1 | 6000 | 91.9 | 6.2 | 80 | |
| | $La_{0.5}Ce_{0.5}$ | 1.8 | 400 | 1 | 6000 | 90 | 5.9 | | |
| | $La_1$ | 1.8 | 400 | 1 | 6000 | 43.9 | 2.9 | 139 | |
| | $La_2O_3$ | 4.8 | 450 | 1 | 18,000 | 58.2 | 11.7 | 41.55 | Huang et al. |
| | $La_2O_3$–K | 4.8 | 450 | 1 | 18,000 | 72.8 | 14.6 | 34.71 | [22] |
| CNT | MWCNT | 5Ru, 10 K | 400 | 1 | 9000 | 30.8 | 2.66 | | Sayas et al. [23] |
| | CNT | 7 | 400 | | 6000 | 12.6 | | 103.8 | Hu et al. [27] |
| $Al_2O_3$ | $Al_2O_3$ | 0.74 | 450 | | 30,000 | | 4.3 | 136.2 | Xu et al. |
| | $Al_2O_3$ | 0.74 | 450 | | 300,000 | | 41.6 | | [19] |
| | γ-$Al_2O_3$ | 1.1 | 380 | 1 | 20,000 | 65 | | 190.8 | Qiu et al. [24] |
| | α-$Al_2O_3$ | 1.3 | 400 | 1 | 60,000 | 22 | 5.07 | 83 | Kim et al. [25] |
| | κ-$Al_2O_3$ | 1 | 400 | 1 | 60,000 | 15 | 2.3 | 103 | Kim et al. |
| | θ-$Al_2O_3$ | 1 | 400 | 1 | 60,000 | 10 | 1.5 | 106 | [25] |
| | κ-$Al_2O_3$ (C300) | 1 | 400 | 1 | 60,000 | 40 | 7 | 65.9 | |
| | θ-$Al_2O_3$ (C300) | 1 | 400 | 1 | 60,000 | 40 | 6.9 | 98.2 | |
| | $Al_2O_3$ | 1.1 | 350 | 1 | 22,000 | | 0.83 | | Hu et al. [26] |
| | $Al_2O_3$ | 7 | 400 | | 6000 | 23 | | 110.8 | Hu et al. [27] |
| $CeO_2$ | $CeO_2$ | 7 | 400 | 1 | 6000 | 85.5 | | 82.5 | Hu et al. [27] |
| | $CeO_2$ | 1 | 450 | 1 | 228,000 | | 99.24 | | Hu et al. |
| | $CeO_2$ | 1 | 450 | 1 | 124,000 | | 83.03 | 150.7 | [26] |
| | $CeO_2$ | 1 | 340 | 1 | 110,000 | | 16.18 | 150.7 | |
| | $CeO_2$ | 1 | 350 | 1 | 22,000 | 32 | 8.14 | 150.7 | |
| | $CeO_2$ | 1 | 300 | 1 | 22,000 | 9 | 2.03 | 150.7 | |
| | $CeO_2$ | 5.1 | 400 | 1 | 2000 | 90 | | 167 | Furusawa et al. [28] |
| | $CeO_2$ | 1 | 450 | | 30,000 | | 1.446 | | Xu et al. [19] |
| | $CeO_2$-I | 1 | 400 | 1 | 22,000 | | 0.91 | | Hu et al. [26] |
| | $CeO_2$ | 1 | 450 | | 300,000 | | 1.266 | | Xu et al. [19] |
| Mg-based | MgO | 1 | 380 | 1 | 20,000 | 68 | | 212.1288 | Qiu et al. [24] |
| | MgO | 1 | 350 | 1 | 22,000 | | 2.54 | | Hu et al. |
| | MgO | 1 | 450 | 1 | 22,000 | 75 | 18.57 | | [26] |
| | MgOa | 3.5 | 450 | 1 | 36,000 | | 11.25 | | |
| | $MgAl_2O_4$ | 0.78 | 350 | 1 | 20,000 | 65 | | 158.992 | Qiu et al. [24] |
| | MgAl | 2 | 450 | 1 | 30,000 | 38 | 12 | 71.7 | Shin et al. [29] |
| | MgO | 5Ru, 10 K | 400 | 1 | 9000 | 39.4 | 3.36 | | Sayas et al. [23] |
| carbon xerogels | CX | 1.35 | 350 | 1 | 2000 | | | 102.6 | Mazzone et al. |
| | ACX 1 h | 1.32 | 350 | 1 | 2000 | | | 82.3 | [30] |
| | ACX 5 h | 1.37 | 350 | 1 | 2000 | | | 93.3 | |
| | UCX | 1.36 | 350 | 1 | 2000 | | | 81.9 | |
| | Na-CX | 1.38 | 350 | 1 | 2000 | | | 88.2 | |
| | Na-ACX 1 h | 1.42 | 350 | 1 | 2000 | | | 76.1 | |
| | Na-ACX 5 h | 1.32 | 350 | 1 | 2000 | | | 90.9 | |
| | Na-UCX | 1.34 | 350 | 1 | 2000 | | | 80.2 | |
| others | NS | 5Ru, 10 K | 400 | 1 | 9000 | 46.6 | 3.91 | | Sayas et al. |
| | CaO | 5Ru, 10 K | 400 | 1 | 9000 | 53.7 | 4.74 | | [23] |

(continued on next page)

**Table 3** (*continued*)

| Name | Support | Loading [wt%] | *T* [°C] | *P* [bar] | *GHSV* [mL $h^{-1}$ $g_{cat}^{-1}$] | $NH_3$ *conversion* [%] | $H_2$ *production rate* [mmol $min^{-1}$ $g_{cat}^{-1}$] | $E_{app}$ [kJ/mol] | References |
|---|---|---|---|---|---|---|---|---|---|
| | $SiO_2$ | 3.64 | 450 | 1 | 30,000 | | 5.9 | 108 | Zhinqiang et al. |
| | $Li_2SiO_3$ | 3.42 | 450 | 1 | 30,000 | 31.2 | 10.4 | 97.1 | [31] |
| | $Na_2SiO_3$ | 3.58 | 450 | 1 | 30,000 | 53.5 | 17.8 | 92.4 | |
| | $K_2SiO_3$ | 3.21 | 450 | 1 | 30,000 | 60.5 | 20.3 | 73.3 | |
| | $TiO_2$ | 2.5 | 500 | | 30,000 | 34.3 | 11.5 | 49.8 | Yan et al. |
| | $TiO_2$-500N-6h | 2.5 | 500 | | 30,000 | 17.8 | 6 | 90.7 | [32] |
| | Ba-$ZrO_2$ | 3 | 500 | | 30,000 | 23.6 | 7.9 | 92.1 | Wang et al. |
| | Ba-$ZrO_2$ | 3 | 500 | | 30,000 | 32.5 | 10.9 | 70.7 | [33] |
| | Ba-$ZrO_2$ | 3 | 500 | | 30,000 | 37.8 | 12.7 | 64.2 | |

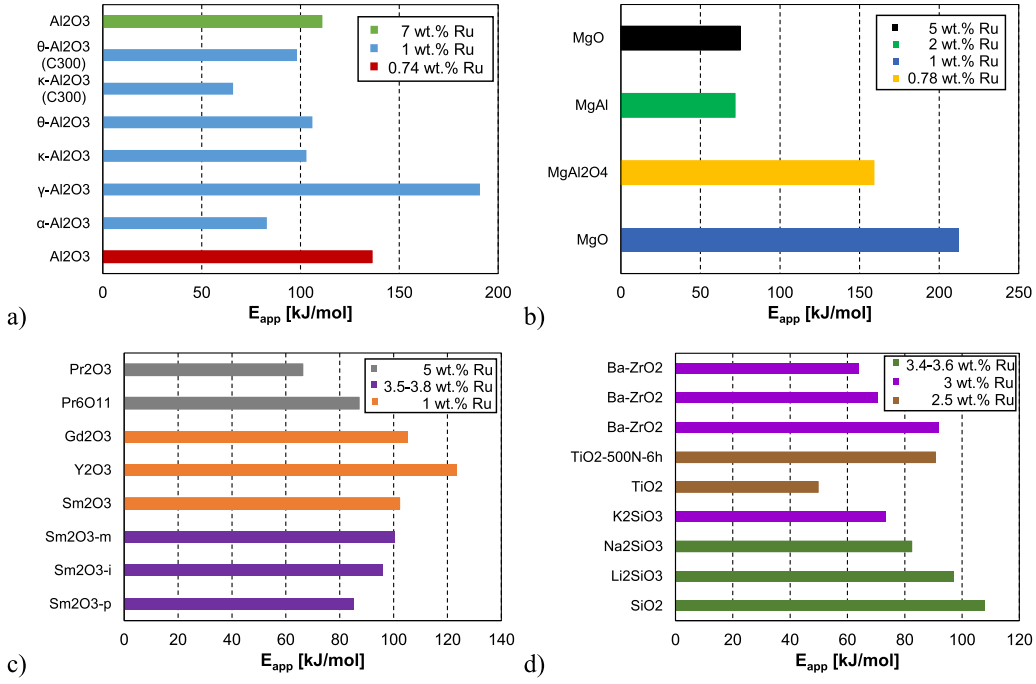


**Fig. 3.** Apparent activation energy ($E_{app}$) of: a) $Al_2O_3$ supported; b) Mg supported; c) rare earth supported d) others Ru-based catalysts of Table 3.

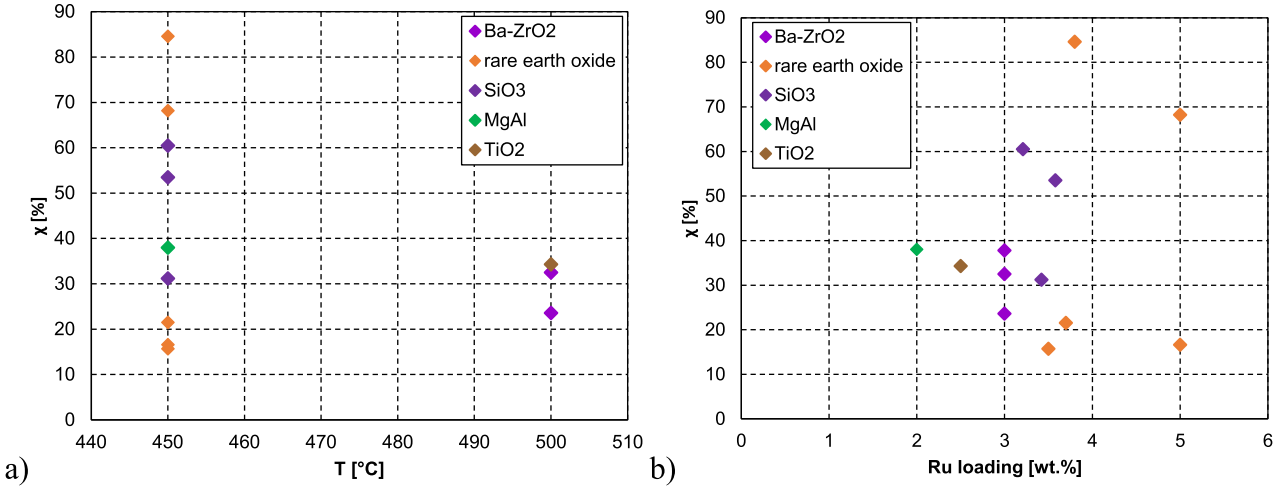


**Fig. 4.** $NH_3$ conversion ($\chi$) for some of the Ru-based catalysts of Table 3 explored in literature, as a function of: a) temperature (*T*) and b) Ru-loading. *GHSV* is fixed at 30,000 mL $h^{-1}$ $g_{cat}^{-1}$.

based catalysts as a function of temperature (*T*) and considering two pressure levels: atmospheric and 40 bar. A benchmark Ni/$Al_2O_3$ catalyst is also included for the sake of comparison.

As illustrated in Fig. 5, the benchmark Ni/$Al_2O_3$ catalyst exhibits significantly lower catalytic activity in $NH_3$ decomposition compared to all other evaluated systems. In contrast, the Ni/$BaAl_2O_3$ catalyst

**Table 4**
Rate expressions of $NH_3$ cracking for Ni- and Ru-based catalysts of, respectively, Tables 2 and 3.

| Active phase | Support | Rate expression | Parameters | | | Reference |
|---|---|---|---|---|---|---|
| | | | $E_{att}$ [kJ/mol] | α | $\beta$ | |
| Ni | Mg-Al-O | $r = k_0 e^{-E_a/RT} P_{NH_3}^{\alpha} P_{H_2}^{\beta}$ | 89.3 | 0.39 | -0.62 | Im et al. [12] |
| | Ca-Al-O | | 87.2 | 0.7 | -0.47 | |
| | Sr-Al-O | | 81.1 | 0.58 | -0.38 | |
| | Ba-Al-O | | 76.5 | 0.47 | -0.37 | |
| Ru | CaO (3 %Ru) | $r = k_0 e^{\frac{-E_a}{RT}} P_{NH_3}^{\alpha} P_{H_2}^{\beta} \left(1 - \frac{1}{K_{eq}} \left(\frac{P_{N_2} P_{H_2}^{\ 3}}{P_{NH_3}^{\ 2}}\right)\right)$ | 96 | 0.8 | -1.9 | Sayas et al. [23] |
| | CaO (3 %Ru10 %K) | | 75 | 0.5 | -1.2 | |
| | $TiO_2$ | $r = k_0 e^{-E_a/RT} P_{NH_3}^{\alpha} P_{H_2}^{\beta}$ | 49.8 | 0.32 | -0.71 | Yan et al. [32] |
| | $TiO_2$-500N-6h | | 90.7 | -0.16 | -0.19 | |
| | $Al_2O_3$ | $r = k_0 e^{-E_a/RT} P_{NH_3}^{\alpha} P_{H_2}^{\beta}$ | 190.8 | 1 | -1.5 | Qiu et al. [24] |
| | MgO | | 212.1 | 1 | -1.5 | |
| | $MgAl_2O_4$ | | 159.0 | 1 | -1.5 | |

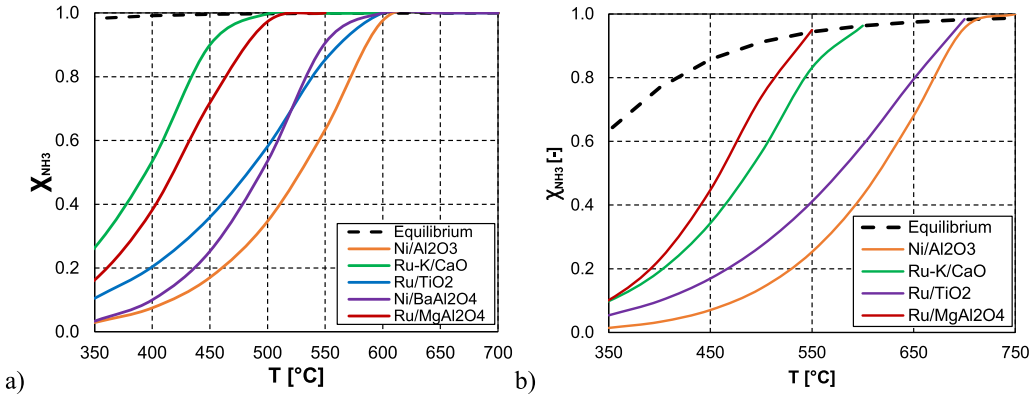


**Fig. 5.** $NH_3$ conversion ($\chi$) for Ni- and Ru-based catalysts as a function of temperature ($T$) at: a) atmospheric pressure and b) 40 bar, considering the rate expressions of Table 4 and a $Ni/Al_2O_3$ benchmark cracking catalyst.

demonstrates markedly improved performance in comparison with the benchmark, confirming that the enhanced basicity of the $BaAl_2O_3$ support contributes positively to $NH_3$ cracking activity, as it facilitates the catalytic cleavage of the N–H bonds. The positive effect of basic promoters is also evident in the case of Ru-K/CaO, which achieves high $NH_3$ conversion efficiencies even at relatively low reaction temperatures ($T = 450$ °C): the synergy between the Ru active phase and the highly basic CaO support, further promoted by potassium, effectively enhances the reaction kinetics.

At elevated pressures the $NH_3$ decomposition reaction becomes less favourable both thermodynamically and kinetically. Despite these constraints, the Ru-K/CaO catalyst maintains superior $NH_3$ conversion performance even at 40 bar (see Fig. 5b).

It should be noted that the $Ni/BaAl_2O_3$ catalyst is not represented in Fig. 5b, as the proposed kinetic model fails to accurately predict $NH_3$ conversion under pressures above atmospheric conditions.

For the development of economically viable $NH_3$ cracking, the maximum acceptable catalyst cost plays a crucial role. In this respect, a preliminary techno-economic analysis can provide a critical framework for identifying performance trade-offs in catalyst selection. Ru-based catalysts can be a promising choice for $NH_3$ cracking, particularly when high purity $H_2$ is needed for downstream mobility applications. Nevertheless, the high cost of ruthenium as a raw material must be weighed against its superior ammonia conversion at lower energy expenses with respect to the commercially available nickel-based alternative. Defining an acceptable cost threshold for catalysts helps benchmark commercial viability and directs research toward materials that satisfy both performance and economic targets. To support this, the following section provides a technical assessment of $NH_3$ cracking.

### 2.4. *Technical assessment of $NH_3$ cracking for decentralized $H_2$ application*

In this section, a technical assessment of $NH_3$ cracking technologies is presented, focusing on the analysis of different Ru-based and Ni-based catalysts.

For the sake of comparison, the basis of design must first be established. According to the $NH_3$ value chain depicted in Fig. 6, ammonia produced from renewable energy or natural gas in combination with carbon capture and storage, referred to as green and blue ammonia, respectively, is assumed to be transported to multiple cracking plants located near end-use sites, such as hydrogen refuelling stations and steel industries. Given the distributed nature of hydrogen utilization, these cracking plants are characterized by a small scale.

A typical ammonia cracking process includes the following process steps: ammonia vaporization, cracking, heat recovery and hydrogen separation/purification. To facilitate downstream $H_2$ purification and reduce associated volumes and costs, it is preferable to operate the cracking reactor under pressure, even though this negatively affects reaction kinetics (see Fig. 5). Since ammonia is typically stored and transported as a liquid, at the cracking plant it is pumped to the desired pressure before vaporization, avoiding the need for costly gas compression. Industrially available crackers are reported to operate at pressures between 20 and 40 bar [10].

For this case-study, a plant fed with 15 ton/d of $NH_3$ is considered, representative of a small-scale facility for decentralized hydrogen

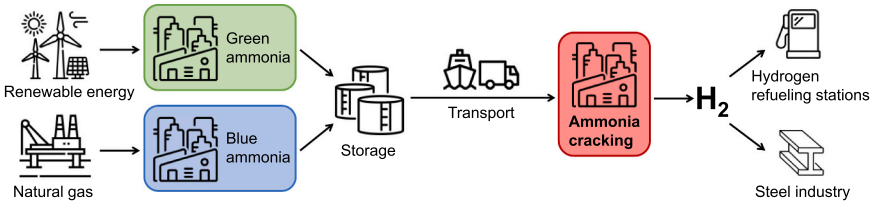


**Fig. 6.** Ammonia value chain.

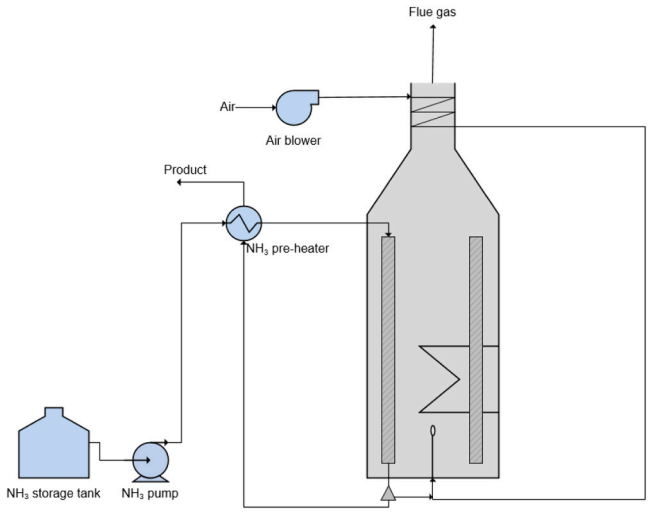


**Fig. 7.** $NH_3$ cracking furnace simplified process flow diagram.

applications. The cracking process is assumed to occur in a fired tubular reactor, operating at 40 bar and achieving an ammonia conversion of 90 %. The downstream hydrogen purification section is not included in this study, as it does not impact on the performance comparison of the different ammonia cracking technologies.

Fig. 7 shows the process flow diagram of the analysed ammonia cracking furnace. A simulation of the furnace reactor has been developed using Aspen Plus® V14, with the PC-SAFT Equation of State selected to model the system under the high-pressure, high-temperature conditions within the furnace. Ammonia from the storage tank, available at 25 °C and 15 bar, is first pressurized to 40 bar and preheated before entering the furnace, which has a cylindrical shape and is equipped with 65 vertical tubes. Each tube is a 1-D pseudo-homogeneous packed bed reactor, with an internal diameter of 0.04 m and a length of 5 m. Different catalyst particles are packed in the tubes, with specifications provided in Table 5. Bed voidage of 0.4 was fixed for all case studies. Further details about the furnace geometry are available in section S2. Pressure drops along the tube are accounted through the Ergun equation, considering a spherical catalyst particle of 0.1 m diameter.

The catalyst-packed tubes are located in the radiant section of the cracking furnace. Radiant and convective heat sources provide the energy required to drive the endothermic cracking reaction, converting most of $NH_3$ into $H_2$ and $N_2$. A portion of this cracked gas is directed to the burner, where it is mixed with preheated combustion air and ignited to supply heat to the furnace. The flow rate of the cracked gas directed to the burner is adjusted to achieve an outlet ammonia conversion of 90 %. Combustion air, available at ambient temperature and pressure, flows through tubes in the convective section at the top of the furnace, exchanging heat with the flue gases. The stack temperature of the flue gases is set at 120 °C. The excess air ratio is controlled to manage the flame temperature, which must remain below 1400 °C to prevent damage to the stainless-steel tubes. The majority of the product gas is routed to the ammonia preheater to enable energy recovery, cooling down significantly before entering downstream separation units for $H_2$ and $N_2$. The approach temperature difference in this heat exchanger is set at 10 °C.

**Table 5**
Specifications of $NH_3$ decomposition catalysts assumed in process simulation.

| Catalyst | Support density [kg/m$^3$] | Catalyst mass [kg] |
|---|---|---|
| 2.8 %Ru9.6 %K/CaO [23] | 3340 | 822 |
| 2.5 %Ru/$TiO_2$ [32] | 4260 | 1072 |
| 0.78 %Ru/$MgAl_2O_4$ [24] | 3600 | 892 |
| 10 %Ni/$Al_2O_3$ [36] | 3970 | 1094 |

## 3. Results and discussions

Referring to the system described in Section 4, Table 6 provides an overview of the results obtained, considering product mass flow, required duty for the cracking reaction to occur and fraction of the cracked product to burner in order to sustain the reaction. The fraction to burner was modified to enable the operating temperature of the system to increase in order to reach 90 % $NH_3$ conversion at the reactor outlet. As a consequence of the fixed $NH_3$ conversion, outlet cracked gas had a composition of 10 wt% $NH_3$, 15.99 wt% $H_2$, 74.02 wt% $N_2$. As the inlet ammonia flow rate is fixed as well as the ammonia conversion, the required duty of Table 6 is a direct indication of the catalytic species performance. K-promoted Ru/CaO shows very similar performance to Ru/$MgAl_2O_4$, the latter with about 1/3 of Ru active phase loading than the former.

In addition, Fig. 8 displays the tube side temperature profiles for all the case-studies. As shown, for the Ni/$Al_2O_3$ case-study, the highest temperature of 700 °C was experienced at the reactor outlet, while, for the Ru/$MgAl_2O_4$, the lowest value of about 580 °C was registered.

To enable a meaningful comparison between the case studies in terms of catalyst's economics and performance, a parameter, $\xi$, is introduced, to account for both capital and operating expenditures. By assuming identical reaction furnace across all simulations (any cost difference due to lower operating temperatures is assumed to be negligible), the primary variation in capital expenses is attributed to the cost of the catalyst. For the Ni-based benchmark, a capital cost of 46 \$/$kg_{cat}$ [37] is assumed, while the expected lifetime is fixed at five years [38]. This cost also includes the metal recovery values and fees.

Regarding the operating expenses, a portion of the unconverted $NH_3$–$H_2$-$N_2$ mixture is utilized as fuel to supply the thermal energy required for the ammonia cracking reaction. Consequently, operating costs are inherently embedded in the net $H_2$ output, thereby simplifying the analysis. On this basis, Eq. (5) is employed to calculate the $\xi$ parameter, which results 0.0158 \$/$kg_{H2}$ for the Ni/$Al_2O_3$ benchmark.

$$\xi = \frac{\frac{CAPEX}{catalystlife}}{H_{2,out}} \quad (5)$$

The ruthenium-based catalyst can emerge as a potentially effective alternative to the nickel-based benchmark if its $\xi$, indication of process economics, is lower or, at most, meets $\xi$ of the latter (see Eq. (6)). To assess this, a breakeven analysis is conducted for each scenario,

**Table 6**
Results for the case-studies analysed.

| case-study | 2.8 %Ru9.6 %K/CaO | 2.5 %Ru/$TiO_2$ | 0.78 %Ru/$MgAl_2O_4$ | Ni/$Al_2O_3$ |
|---|---|---|---|---|
| Product mass flow [kg/h] | 506.4 | 506.2 | 506.4 | 505.3 |
| *Q* [kW] | 700.88 | 705.01 | 699.85 | 714.75 |
| fraction to burner [-] | 0.1897 | 0.1901 | 0.1897 | 0.1916 |

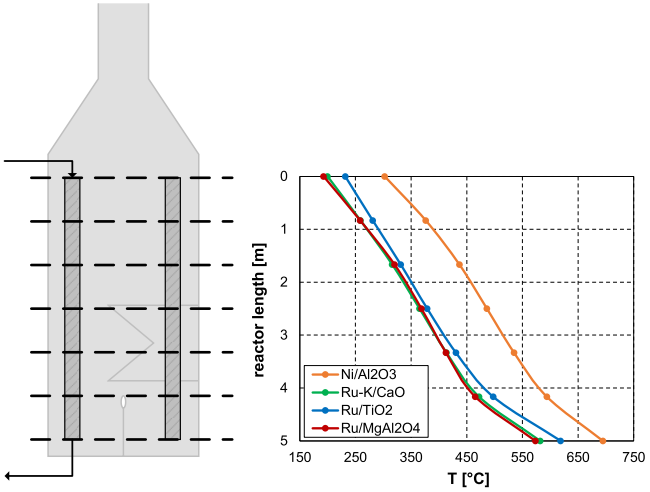


**Fig. 8.** Tube side temperature profiles within the cracking furnace.

considering the hydrogen production flow rate of Table 6. By determining the breakeven point, the analysis offers insight into the feasibility of adopting ruthenium-based catalysts in practical applications, particularly within decentralized hydrogen production systems where performance and cost efficiency must be carefully balanced. Eq. (7) is applied for accounting for the breakeven point and resulting values are reported in Table 7.

$$(\xi)_{Ru-cat} \leq (\xi)_{Ni-cat} \tag{6}$$

$$\left(\frac{CAPEX}{catalystlife}\right)_{Ru-cat} \leq (H_{2,out})_{Ru-cat} \cdot (\xi)_{Ni-cat} \tag{7}$$

To further explore these results, the methodology proposed by Super and mentioned by the National Renewable Energy Laboratory is applied [37,39].

According to this methodology, the Precious Metal Loop is applied to identify catalyst cost, which includes 4 steps: buy the catalyst, make the product, ship spent catalyst to a refiner and receive the Platinum Group Metal (PGM) settlement [40]. For identification of the expenses, assumptions of Table 8 are introduced. Accountability stands for the recovery percentage of the noble metal upon refining. The amount of noble metal not recovered must be reintroduced and this is regarded as a cost in retrieving the overall catalyst expense. The PGM to be reintroduced is credited to the pool account.

As a result, referring to the total catalyst expense to the catalyst mass of Table 8, the catalyst cost [$/kg] can be retrieved. When compared to the nickel-based (Ni-based) system, these costs are significantly higher for the ruthenium-based (Ru-based) alternatives. For the Ru-based alternatives to be economically viable, *i.e.*, to meet the $\frac{CAPEX}{catalystlife}$ ratio of the Ni-benchmark provided in Table 7, their catalyst lifetime must be substantially extended. Specifically, the lifetimes must be increased by factors of 3.4, 2.8 and 1.8 times than Ni-based catalyst for 2.8 %Ru9.6 % K/CaO, 2.5 %Ru/$TiO_2$ and 0.78 %Ru/$MgAl_2O_4$, respectively. Among these options, the Ru/CaO catalyst emerges as the least viable route for practical $NH_3$ cracking, due to its disproportionately high cost-performance ratio, despite its higher $NH_3$ conversion activity. The $MgAl_2O_4$-supported catalyst, which contains the lowest concentration of active metal, presents itself as the most promising candidate from both technical and economic perspectives. The 0.78 %Ru/$MgAl_2O_4$ system stands out as a compelling starting point for future investigations into catalyst design aimed at optimizing performance and reducing overall cost.

## 4. Conclusions

$NH_3$ cracking is garnering increasing attention as a promising route for on-demand, carbon-free hydrogen ($H_2$) production. However, the commercial viability of this process is heavily dependent on the development of highly active, stable, and economically feasible catalytic systems. Among the most extensively studied catalysts are those based on nickel (Ni) and ruthenium (Ru), each offering distinct advantages and limitations.

Ru-based catalysts exhibit outstanding catalytic activity due to favourable Ru–N interactions, which facilitate efficient $NH_3$ decomposition. Nevertheless, the high cost associated with Ru significantly impedes their large-scale deployment. To mitigate this, efforts have focused on reducing Ru content through various strategies, including support engineering, alkali metal doping, and the use of activity-enhancing promoters such as K, Na, and Cs. These approaches aim to maximize catalytic efficiency while minimizing precious metal usage.

Ni-based catalysts, on the other hand, offer a more cost-effective alternative but are generally hindered by lower intrinsic activity and limited long-term stability. Enhancement strategies for Ni systems include transition metal doping, utilization of advanced support materials such as layered double hydroxides and perovskites, and incorporation of rare-earth promoters like Ce, La, and Sr. While these measures have led to noticeable performance improvements, Ni catalysts still lag behind Ru systems in terms of overall efficiency.

To systematically assess the interplay between catalyst performance and economic viability, a techno-economic analysis of $NH_3$ cracking using various catalytic formulations (2.8 %Ru9.6 %K/CaO, 2.5 %Ru/$TiO_2$ and 0.78 %Ru/$MgAl_2O_4$) was conducted. As expected, for Ru-based systems to be competitive with Ni-based benchmark, significantly extended catalyst lifetimes and/or $NH_3$ conversion performance are required. Specifically, the Ru/CaO catalyst necessitates an impractically long lifetime, rendering it unrealistic for commercial application.

Of these, the $MgAl_2O_4$-supported catalyst, characterized by the lowest noble metal loading, emerges as a particularly viable candidate for further development. Its balance of reduced cost and satisfactory

**Table 7**
Process and cost performance indicators for the case studies analysed.

| Case-study | 2.8 %Ru9.6 %K/CaO | 2.5 %Ru/$TiO_2$ | 0.78 %Ru/$MgAl_2O_4$ | Ni/$Al_2O_3$ |
|---|---|---|---|---|
| $\frac{CAPEX}{catalystlife}$[$/y] | 5.2025 | 5.1998 | 5.2023 | 5.1903 |

**Table 8**
Estimation of capital expenses for PGM-based catalysts.

| Assumptions | | Output | | | |
|---|---|---|---|---|---|
| Description | Value | Description | 2.8 %Ru9.6 %K/CaO | 2.5 %Ru/$TiO_2$ | 0.78 %Ru/$MgAl_2O_4$ |
| Ru cost [$/Toz] | 675 [41] | loading [wt%] | 2.8 | 2.5[a] | 0.78 |
| Toz/kg | 32 | dry cat [kg] | 822 | 1072 | 892 |
| Recovery of PGM [%] | 90 [39] | catalyst purchase ex PGM [$] | 46,980 | 39,690 | 36,990 |
| cost of fabrication and support [$/kg] | 45 [37] | PGM make-up [$] | 17,089 | 12,890 | 3748 |
| $kg_{dry\ cat}/kg_{spent\ cat}$ | 8 [39] | | | | |
| *Refining* | | | | | |
| PGM lease [$] | 13,160 [39] | | | | |
| shipping to refine [$] | 2500 [39] | | | | |
| handling charges [$/$kg_{spent\ cat}$] | 2.5 [39] | total refining cost [$] | 173,182 | 27,142 | 20,976 |
| refining fee [$/$Toz_{recovered}$] | 11 [39] | replenish pool account [$] | 80,380 | 60,631 | 17,630 |
| Accountability [%] | 97 [39] | | | | |
| | | total capital expense [$] | 173,182 | 140,623 | 88,756 |
| | | **catalyst cost [$/kg]** | 170 | 156 | 106 |

[a]nominal noble metal loading. The actual Ru content is not provided by reference [32].

activity highlights the critical role of support selection and active phase dispersion in achieving both technical efficiency and economic sustainability.

These results emphasize the necessity of tailoring catalyst design not only for reactivity but also for cost-effectiveness, particularly in applications targeting decentralized or scalable hydrogen production. Future research should prioritize enhancing catalyst durability, further reducing Ru content and exploring alternative supports and promoters.

## CRediT authorship contribution statement

**Pellegrini Laura Annamaria:** Writing – review & editing, Supervision, Methodology, Conceptualization. **Giorgia De Guido:** Writing – review & editing, Supervision. **Stefania Moioli:** Writing – review & editing, Supervision. **Elvira Spatolisano:** Writing – original draft, Methodology, Investigation, Conceptualization. **Federica Restelli:** Writing – review & editing, Software, Methodology.

## Declaration of Competing Interest

The authors declare that they have no known competing financial interests or personal relationships that could have appeared to influence the work reported in this paper.

## Appendix A. Supporting information

Supplementary data associated with this article can be found in the online version at doi:10.1016/j.apcata.2025.120670.

## Data availability

Data will be made available on request.

## References


[1] E. Spatolisano, L.A. Pellegrini, A.R. de Angelis, S. Cattaneo, E. Roccaro, Ammonia as a carbon-free energy carrier: NH3 cracking to H2, Ind. Eng. Chem. Res. 62 (2023) 10813–10827.

[2] E. Spatolisano, F. Restelli, L.A. Pellegrini, S. Cattaneo, A.R. de Angelis, A. Lainati, E. Roccaro, Liquefied hydrogen, ammonia and liquid organic hydrogen carriers for harbour-to-harbour hydrogen transport: a sensitivity study, Int. J. Hydrog. Energy 80 (2024) 1424–1431.

[3] Z. Su, J. Guan, Y. Liu, D. Shi, Q. Wu, K. Chen, Y. Zhang, H. Li, Research progress of ruthenium-based catalysts for hydrogen production from ammonia decomposition, Int. J. Hydrog. Energy 51 (2024) 1019–1043.

[4] I. Lucentini, X. Garcia, X. Vendrell, J. Llorca, Review of the decomposition of ammonia to generate hydrogen, Ind. Eng. Chem. Res. 60 (2021) 18560–18611.

[5] T. Su, B. Guan, J. Zhou, C. Zheng, J. Guo, J. Chen, Y. Zhang, Y. Yuan, W. Xie, N. Zhou, Review on Ru-based and Ni-based catalysts for ammonia decomposition: research status, reaction mechanism, and perspectives, Energy Fuels 37 (2023) 8099–8127.

[6] N. Li, C. Zhang, D. Li, W. Jiang, F. Zhou, Review of reactor systems for hydrogen production via ammonia decomposition, Chem. Eng. J. 495 (2024) 153125.

[7] N. Zhu, F. Yang, Y. Hong, J. Liang, Hydrogen production from ammonia decomposition: Advances in Ru- and Ni-based catalysts, Int. J. Hydrog. Energy 98 (2025) 1243–1261.

[8] BASF, SYNSPIRE™ ARC – Ammonia reforming catalysts, 2025.

[9] T. Davison, J. Ashcroft, Making and breaking NH3 – Ammonia and its place in the low carbon economy. Nitrogen + Syngas Conference, Johnson Matthey, Berlin, Germany, 2022.

[10] Clariant, Catalysts to tackle the challenges of ammonia cracking, Nitrogen+Syngas 384⟨www.nitrogenandsyngas.com⟩, 2023.

[11] P. Brito, H2RetakeTMAmmonia Cracking –TOPSOE's innovative technology. Building on industrial experience., AEA Conference -Ammonia Cracking Session, 2024.

[12] Y. Im, H. Muroyama, T. Matsui, K. Eguchi, Ammonia decomposition over nickel catalysts supported on alkaline earth metal aluminate for H2 production, Int. J. Hydrog. Energy 45 (2020) 26979–26988.

[13] Q.C. Do, Y. Kim, T.A. Le, G.J. Kim, J.-R. Kim, T.-W. Kim, Y.-J. Lee, H.-J. Chae, Facile one-pot synthesis of Ni-based catalysts by cation-anion double hydrolysis method as highly active Ru-free catalysts for green H2 production via NH3 decomposition, Appl. Catal. B Environ. Energy 307 (2022) 121167.

[14] M. Yu, R. Sun, G. Luo, L. Wang, X. Li, H. Yao, Ammonia partial cracking over low-cost Ni catalysts for enhancing combustion, Fuel 367 (2024) 131306.

[15] X.-Y. Guo, J.-H. Wang, Q. Zhang, T.-Z. Li, H. Dong, C.-J. Jia, C. Li, Y.-W. Zhang, Alkaline Earth metal promoted hydrogen production from ammonia decomposition over Ni/La2O3-based catalysts, Appl. Catal. B Environ. Energy 348 (2024) 123844.

[16] T. Kocer, F.E. Saraç-Öztuna, S.F. Kurtoğlu-Öztulum, U. Unal, A. Uzun, Effect of Nickel precursor on the catalytic performance of graphene aerogel-supported nickel nanoparticles for the production of COx-free hydrogen by ammonia decomposition, Energy Technol. 10 (2022) 2100794.

[17] Z.-P. Hu, C.-C. Weng, C. Chen, Z.-Y. Yuan, Catalytic decomposition of ammonia to COx-free hydrogen over Ni/ZSM-5 catalysts: A comparative study of the preparation methods, Appl. Catal. A Gen. 562 (2018) 49–57.

[18] X. Zhang, L. Liu, J. Feng, X. Ju, J. Wang, T. He, P. Chen, Metal–support interaction-modulated catalytic activity of Ru nanoparticles on Sm 2 O 3 for efficient ammonia decomposition, Catal. Sci. Technol. 11 (2021) 2915–2923.

[19] K. Xu, J.-C. Liu, W.-W. Wang, L.-L. Zhou, C. Ma, X. Guan, F.R. Wang, J. Li, C.-J. Jia, C.-H. Yan, Catalytic properties of trivalent rare-earth oxides with intrinsic surface oxygen vacancy, Nat. Commun. 15 (2024) 5751.

[20] X. Zhang, L. Liu, J. Feng, X. Ju, J. Wang, T. He, P. Chen, Ru nanoparticles on Pr2O3 as an efficient catalyst for hydrogen production from ammonia decomposition, Catal. Lett. 152 (2022) 1170–1181.

[21] T.A. Le, Y. Kim, H.W. Kim, S.-U. Lee, J.-R. Kim, T.-W. Kim, Y.-J. Lee, H.-J. Chae, Ru-supported lanthania-ceria composite as an efficient catalyst for COx-free H2 production from ammonia decomposition, Appl. Catal. B Environ. 285 (2021) 119831.

[22] C. Huang, Y. Yu, J. Yang, Y. Yan, D. Wang, F. Hu, X. Wang, R. Zhang, G. Feng, Ru/La2O3 catalyst for ammonia decomposition to hydrogen, Appl. Surf. Sci. 476 (2019) 928–936.

[23] S. Sayas, N. Morlanés, S.P. Katikaneni, A. Harale, B. Solami, J. Gascon, High pressure ammonia decomposition on Ru–K/CaO catalysts, Catal. Sci. Technol. 10 (2020) 5027–5035.

[24] Y. Qiu, F.S. Franchi, N. Usberti, A. Beretta, Kinetic Investigation of Nh3 Decomposition Over Ru-Based Catalysts: The Limiting Role of H* Surface Coverage Demonstrated by Experiments and Modelling, Available at SSRN 4923910.

[25] H.B. Kim, E.D. Park, Ammonia decomposition over Ru catalysts supported on alumina with different crystalline phases, Catal. Today 411 (2023) 113817.

[26] X.-C. Hu, X.-P. Fu, W.-W. Wang, X. Wang, K. Wu, R. Si, C. Ma, C.-J. Jia, C.-H. Yan, Ceria-supported ruthenium clusters transforming from isolated single atoms for hydrogen production via decomposition of ammonia, Appl. Catal. B Environ. 268 (2020) 118424.
[27] Z. Hu, J. Mahin, S. Datta, T.E. Bell, L. Torrente-Murciano, Ru-based catalysts for H 2 production from ammonia: effect of 1D support, Top. Catal. 62 (2019) 1169–1177.
[28] T. Furusawa, H. Kuribara, K. Kimura, T. Sato, N. Itoh, Development of a Cs-Ru/CeO2 spherical catalyst prepared by impregnation and washing processes for low-temperature decomposition of NH3: characterization and kinetic analysis results, Ind. Eng. Chem. Res. 59 (2020) 18460–18470.
[29] J. Shin, U. Jung, J. Kim, K.D. Kim, D. Song, Y. Park, B.-S. An, K.Y. Koo, Elucidating the effect of Ce with abundant surface oxygen vacancies on MgAl2O4-supported Ru-based catalysts for ammonia decomposition, Appl. Catal. B Environ. 340 (2024) 123234.
[30] S. Mazzone, T. Goklany, G. Zhang, J. Tan, E.I. Papaioannou, F.R. García-García, Ruthenium-based catalysts supported on carbon xerogels for hydrogen production via ammonia decomposition, Appl. Catal. A Gen. 632 (2022) 118484.
[31] F. Zhiqiang, W. Ziqing, L. Dexing, L. Jianxin, Y. Lingzhi, W. Qin, W. Zhong, Catalytic ammonia decomposition to COx-free hydrogen over ruthenium catalyst supported on alkali silicates, Fuel 326 (2022) 125094.
[32] W. Yan, W. Wang, Q. Gu, B. Zhang, G. Bi, H. Zhuo, X. Shang, G. Xu, F. Wang, T. Zhang, Interfacial evolution of Ru/TiO2 catalysts in NH3 decomposition, J. Energy Chem. (2025).
[33] Z. Wang, Y. Qu, X. Shen, Z. Cai, Ruthenium catalyst supported on Ba modified ZrO2 for ammonia decomposition to COx-free hydrogen, Int. J. Hydrog. Energy 44 (2019) 7300–7307.
[34] A. Takahashi, T. Fujitani, Kinetic analysis of decomposition of ammonia over Nickel and Ruthenium catalysts, J. Chem. Eng. Jpn. 49 (2016) 22–28.
[35] S. Sun, Q. Jiang, D. Zhao, T. Cao, H. Sha, C. Zhang, H. Song, Z. Da, Ammonia as hydrogen carrier: Advances in ammonia decomposition catalysts for promising hydrogen production, Renew. Sustain. Energy Rev. 169 (2022) 112918.
[36] K. Okura, T. Okanishi, H. Muroyama, T. Matsui, K. Eguchi, Ammonia decomposition over Nickel catalysts supported on rare-earth oxides for the on-site generation of hydrogen, ChemCatChem 8 (2016) 2988–2995.
[37] F.G. Baddour, L. Snowden-Swan, J.D. Super, K.M. Van Allsburg, Estimating precommercial heterogeneous catalyst price: a simple step-based method, Org. Process Res. Dev. 22 (2018) 1599–1605.
[38] S. Richard, A. Ramirez Santos, P. Olivier, F. Gallucci, Techno-economic analysis of ammonia cracking for large scale power generation, Int. J. Hydrog. Energy 71 (2024) 571–587.
[39] J.D. Super, The precious metal loop, costs from an operating company perspective, Top. Catal. 53 (2010) 1138–1141.
[40] L. Cline, Precious Met. Recovery Precious Met. 'Loop' (2017) 71–80.
[41] J. Matthey, PGM management, 2025.